Enhancing Bearing Fault Diagnosis in Induction Motors: A Novel Approach Leveraging Synchronized Deviation of Instantaneous Frequency of Voltage and Current

Somaye Nazari[1,*], Jamal Moshtagh[2]

[1]PhD Candidate, Electrical Engineering Department, University of Kurdistan, Sanandaj, Iran
[2]Professor, Electrical Engineering Department, University of Kurdistan, Sanandaj, Iran

Abstract:

Current-based methods for bearing fault diagnosis primarily rely on analyzing the current signal, leading to challenges in detecting fault frequencies due to their low magnitude amid the noise in the current spectrum. This issue intensifies for weak bearing faults in their early stages. The presence of noise components increases the risk of false alarms, as fault characteristics are often obscured in the raw current spectral analysis. To address this, effective bearing fault diagnosis necessitates the reduction of noise components. This paper presents a novel noise cancellation method that enhances the estimation of bearing fault signals in induction motors by utilizing the deviation of instantaneous frequency in synchronized motor voltage and current signals. The proposed method efficiently diagnoses bearing fault characteristic frequencies during spectral analysis. Simulation and experimental results substantiate the effectiveness of this approach in detecting outer/inner raceway and ball bearing faults.

Keywords:

Bearing Fault Diagnosis, Instantaneous Frequency, Induction Motor, Noise Reduction.

* Corresponding author, E-mail: s.nazari@uok.ac.ir

1. Introduction

Fault diagnosis in bearings constitutes a critical aspect of condition monitoring and predictive maintenance across diverse industrial applications. Bearings are pivotal in ensuring the proper functioning of rotating machinery, such as motors, pumps, and turbines. Over time, factors like wear, misalignment, or contamination can give rise to bearing issues. If left undetected, these issues may lead to reduced efficiency, increased downtime, and, in extreme scenarios, catastrophic failure. Traditionally, the bearing fault diagnosis heavily relies on vibration analysis, involving the measurement and examination of mechanical vibrations generated by rotating equipment. However, in recent years, there has been a growing interest in utilizing electrical signals, particularly stator currents, for bearing fault detection [1-5]. The condition of the bearings directly influences the electrical signals generated by the motor. When bearing faults occur, they introduce irregularities in the motion of the rotating shaft, affecting the magnetic field and subsequently altering the stator currents. These deviations in electrical signals contain valuable information about the presence and severity of bearing faults. Using electrical signals for bearing fault diagnosis offers several advantages over traditional vibration-based methods. One significant advantage is the ability to detect faults in their early stages, allowing maintenance teams to proactively implement measures to prevent further deterioration [6]. Furthermore, electrical signal analysis can provide deeper insights into the root causes of bearing faults, facilitating improved fault classification and an understanding of the underlying mechanisms.

In a pioneering effort, [7] investigates the utilization of stator current monitoring for the identification of motor bearing damage. The authors examine alterations in stator current patterns induced by bearing faults and propose a methodology for discerning specific fault signatures. This study underscores the potential of stator current analysis as a non-intrusive technique for the early detection of bearing faults. Another innovative approach for detecting faults in induction motors (IMs) is presented in [8]. This study focuses on the analysis of the space vector representation of motor current signals to pinpoint and diagnose misalignment and bearing faults. In [9], Bouras and colleagues employ fast Fourier transform

(FFT) spectral analysis, complemented by the Park vector, to extract bearing fault characteristics from current signals. Within the category of signal feature extraction research, distinctive features of the fault signal are isolated from the measured signal content. Techniques within this category encompass wavelet packet decomposition [10, 11], spectral kurtosis [12, 13], and empirical mode decomposition [14]. In another category of research, researchers have endeavored to enhance the signal-to-noise ratio (SNR) through methods such as Gaussian noise reduction [7], filter design [15-17], time shifting [1, 2], and linear prediction [3, 18]. In [19], a time-shift denoising and a discrete wavelet transform enhanced conditional domain adaptation framework is utilized. In [20], the IM current signal is subjected to a wavelet filter with a soft-hard threshold to eliminate the noise. Then, the processed data is fed as input to a one-dimensional neural network to diagnose rolling bearing faults. [21] presents an innovative method for bearing fault diagnosis, emphasizing current noise reduction using a model-based approach with a Luenberger observer. These methods aim to improve the detection of bearing fault characteristics in the frequency spectrum.

There have been few studies exploring the use of various electrical signals for bearing fault detection. These signals encompass the instantaneous power factor [22] and the instantaneous frequency of motor voltage (IFMV) [23, 24] signals. In [24], for the first time, the impact of bearing faults on stator voltage has been empirically established, and the IFMV signal has been introduced as a novel signal for detecting bearing faults. This signal identifies the presence of bearing faults in the time domain by utilizing statistical indicators like global kurtosis. However, it has encountered limitations in pinpointing specific types of bearing faults and identifying fault characteristic frequencies in the frequency domain.

In this paper, a novel method for bearing fault diagnosis is proposed, relying on the synchronized deviation of the instantaneous frequency of voltage and current to generate a residue for bearing fault diagnosis purposes. The primary idea behind the proposed method in this paper stems from the unique characteristics of the IM, where, due to specific self-inductance properties within its coil windings, the current signal exhibits a phase difference with the voltage signal. Consequently, in transient states,

mechanical faults can affect the current and voltage signals with a phase difference (time shifting) equal to the phase difference between both. Given the minimal impact of faults on the voltage signal, previous works [23, 24] have relied solely on statistical indices and time-domain analysis for fault detection using IFMV signal, failing to identify the fault characteristic frequency in the frequency domain. Unfortunately, they were unable to identify the characteristic fault frequency in the frequency domain analysis, primarily due to the low magnitude of the fault characteristic frequency and its overshadowing by noise in the frequency spectrum. In this paper, an attempt has been made to synchronize the effects of the bearing fault on the IFMV signal with the effects of the bearing fault on the instantaneous frequency of the motor current (IFMC) signal by time-shifting the IFMV signal and then to perform spectral analysis on the deviation of IFMC and IFMV signals. In fact, in the rest of the paper, it is proven that the proposed deviation signal, named residue, can greatly reduce the noises, and help to better see the fault characteristic frequency in the frequency analysis. In essence, the proposed residue reduces the magnitude of non-fault components, thereby enhancing the SNR and enabling the detection of the specific type of bearing fault. Importantly, this method does not necessitate additional sensors and solely utilizes information already available from the stator voltage and current. The proposed method undergoes testing under various load conditions and for three types of bearing faults: outer raceway (with two severity levels), inner raceway, and ball faults. The key advantages of this bearing fault detection method are as follows:

- *Introduction of a novel signal for bearing fault diagnosis.*

- *Presentation of a systematic noise reduction technique using the proposed residue in place of a portion of the signal conditioning process in bearing fault diagnosis approaches.*

The remainder of this paper is organized as follows: Section III outlines the overall structure of the proposed bearing fault detection approach. Section IV conducts a simulation test to validate the effectiveness of the proposed method. In Section V, the experimental setup employed in this study is

elucidated, and subsequent experimental results are presented, illustrating the efficacy of the proposed

diagnostic approach under various faulty conditions (outer raceway, inner raceway, and ball faults on the

bearing), different operating points of an IM, and two levels of fault severity (low-level and high-level).

Finally, Section VI presents the conclusions.

2. Proposed Bearing Fault Diagnosis Method

In this section, an explanation of the overall structure of the proposed method is provided.

2-1- Instantaneous Frequency of Motor Voltage and Current

The typical structure of a ball bearing is depicted in Fig. 1. Its main components include the inner

raceway, outer raceway, and ball elements. To prevent contact between the balls and to maintain uniform

spacing, a cage encases the ball elements. Industrial bearing faults are generally categorized into two

types: single-point faults and generalized roughness faults [25]. A "single-point fault" refers to a localized

defect, such as a pit or spall, on the bearing surface, often caused by overloading during operation. On the

other hand, a "generalized roughness fault" involves surface roughening and deformation, typically

resulting from factors such as insufficient lubrication, misalignment, or contamination [23]. This study

focuses exclusively on "single-point faults." When a fault occurs in any bearing component, it generates a

specific frequency characteristic of that component. These fault frequencies are determined by the

bearing's geometry and operating speed [32]. The frequency characteristics of such faults are outlined as

follows:

$$
\begin{cases}
F_O = \dfrac{N_B}{2} F_R \left(1 - \dfrac{D_b \cos\beta}{D_c} \right) \\[2ex]
F_I = \dfrac{N_B}{2} F_R \left(1 + \dfrac{D_b \cos\beta}{D_c} \right) \\[2ex]
F_B = \dfrac{D_c}{2D_b} F_R \left(1 - \left(\dfrac{D_b \cos\beta}{D_c} \right)^2 \right)
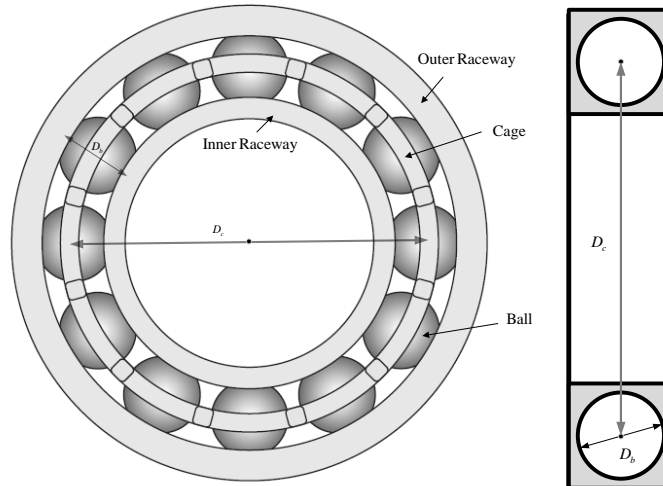\end{cases}
\tag{1}
$$

Fig. 1. Common configuration of a ball bearing

Here, F_R, F_I, F_O, and F_B denote the rotor mechanical frequency, inner raceway fault frequency, outer raceway fault frequency, and ball fault frequency, respectively. D_c represents the pitch diameter, D_b is the ball diameter, N_B refers to the number of ball elements, and β is the ball contact angle. In this study, the motor bearings used are type 6309, which contain 8 balls. The pitch diameter D_c and ball diameter D_b are 74.0mm and 17.2mm, respectively. The ball contact angle β is assumed to be zero ($\cos\beta=1$). Consequently, the fault frequencies for the type 6309 bearing are calculated using (1) as $F_O = 3.06\times F_R$, $F_I = 4.95\times F_R$, and $F_B = 2.00\times F_R$.

In [7], the connection between the distinctive frequencies associated with bearing faults in vibration and stator current signals is articulated as follows:

$$f_{\text{i-bg}} = \left| f_s \mp k f_{v\text{-}bg} \right| \tag{2}$$

here, $k=1,2,3, \ldots$ and $f_{i\text{-}bg}$, $f_{v\text{-}bg}$ and f_s represent the current harmonic due to the faulty bearing, the vibration characteristic frequency due to the faulty bearing, and the fundamental supply current frequency, respectively. Therefore, in the case of an IM with a bearing fault, the stator current can be depicted as follows (without taking Gaussian noise into account) [1]:

$$I_F(t) = I_m \cos(\omega_s t - \alpha) + \sum_{k=1}^{\infty} I_k \cos((\omega_s \pm k\omega_f)t - \alpha) \tag{3}$$

where, α is current angle. $\omega_s = 2\pi f_s$ and $\omega_f = 2\pi f_{v-bg}$ are the angular speed of the power supply and the bearing fault characteristic, respectively. Now, let's contemplate the equivalent circuit of a squirrel cage IM, illustrated in Fig. 2. To simplify the calculations, we only consider the first component of the fault current in Eq. (3) (where $k=1$):

$$I_F(t) = I_m \cos(\omega_s t - \alpha) + I_1 \cos((\omega_s - \omega_f)t - \alpha) + I_1 \cos((\omega_s + \omega_f)t - \alpha). \tag{4}$$
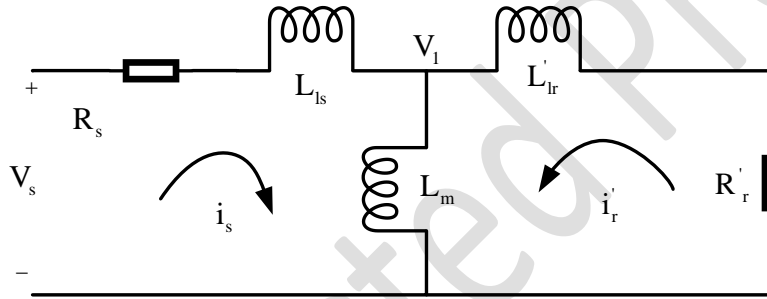

Fig. 2. Equivalent circuit of a squirrel cage IM.

Following the application of Kirchhoff's voltage law (KVL) and Kirchhoff's current law (KCL), the stator voltage is derived as follows:

$$
\begin{aligned}
V_s(t) = ze^{-\frac{r'}{L'_{lr}+L_m}t} &+ G\sin(\omega_s t - \alpha) + H\cos(\omega_s t - \alpha) + I\sin((\omega_s - \omega_f)t - \alpha) + J\cos((\omega_s - \omega_f)t - \alpha) \\
&+ K\sin((\omega_s + \omega_f)t - \alpha) + L\cos((\omega_s + \omega_f)t - \alpha)
\end{aligned}
\tag{5}
$$

In this equation, the coefficients z, G, H, I, J, K, and L are detailed in the appendix. It's important to note that under steady-state conditions, the first term of Eq. (5) becomes zero.

As outlined in [23], the IFMV signal is derived from the following equation:

$$IFMV(t) = \frac{1}{2\pi}\frac{d}{dt}\varphi_{V_s}(t) \tag{6}$$

where, $\varphi_{\bar{V}_s}$ is the phase of the analytical signal $\bar{V}_s(t)$:

$$\bar{V}_s(t) = V_s(t) + jV_H(t) \tag{7}$$

here, $V_H(t)$ is the Hilbert transform of $V_s(t)$ and can be obtained from Eq. (5) as follows:

$$
\begin{aligned}
V_H(t) = &-G\cos(\omega_s t - \alpha) + H\sin(\omega_s t - \alpha) - I\cos((\omega_s - \omega_f)t - \alpha) + J\sin((\omega_s - \omega_f)t - \alpha) \\
&- K\cos((\omega_s + \omega_f)t - \alpha) + L\sin((\omega_s + \omega_f)t - \alpha)
\end{aligned}
\tag{8}
$$

Finally, the frequency is obtained as follows:

$$
IFMV(t) = \frac{1}{2\pi \times d(t)}
\begin{pmatrix}
M + N\cos((2\omega_s - \omega_f)t - 2\alpha) \\
+ O\cos((2\omega_s + \omega_f)t - 2\alpha) \\
+ P\cos(2\omega_s t - 2\alpha) \\
+ Q\sin(\omega_f t) + R\sin(2\omega_f t)
\end{pmatrix}
\tag{9}
$$

In a manner like Eq. (6) through Eq. (8), and by utilizing Eq. (4), the IFMC is calculated as follows:

$$
IFMC(t) = \frac{1}{2\pi \times d'(t)}
\begin{pmatrix}
M' + N'\cos((2\omega_s - \omega_f)t) \\
+ O'\cos((2\omega_s + \omega_f)t) \\
+ P'\cos(2\omega_s t)
\end{pmatrix}
\tag{10}
$$

where, functions $d(t)$ and $d'(t)$ and coefficients $M, M', N, N', O, O', P, P', Q,$ and R are included in the Appendix.

Notably, Eq. (9) and Eq. (10) do not account for measurement noise. It is evident from these equations that the fault characteristic frequency is discernible in the IFMV but not in the IFMC. When measurement noise is introduced into Eq. (9), the magnitude of the fault characteristic frequency can potentially become obscured within the existing noise spectrum. This may explain why [23] encountered challenges in diagnosing the fault type based on the IFMV frequency spectrum. In the subsequent sections, an effort is made to enhance the SNR by synchronizing the IFMV and IFMC signals. This synchronization aims to

mitigate the impact of background noise and non-fault signal components, consequently improving the SNR.

In the discrete-time domain and assuming rapid sampling, the calculations for IFMV and IFMC are as follows [23]:

$$IFMV[m] = \frac{1}{2\pi} \frac{(V_H[m]V_s[m-1] - V_H[m-1]V_s[m])}{(t[m] - t[m-1])|\bar{V}_s[m]||\bar{V}_s[m-1]|} \tag{11}$$

$$IFMC[m] = \frac{1}{2\pi} \frac{(I_H[m]I_s[m-1] - I_H[m-1]I_s[m])}{(t[m] - t[m-1])|\bar{I}_s[m]||\bar{I}_s[m-1]|}. \tag{12}$$

In these equations, V_s and I_s denote the stator voltage and current, while t signifies time. The indices m and H refer to the mth sample and the Hilbert transform, respectively.

2-2- General Framework of the Proposed Method for Diagnosing Bearing Faults

Fig. 3 illustrates the comprehensive framework of the proposed approach for bearing fault diagnosis. To commence the process, the motor's voltage and current data are acquired using the voltage and current transformers (PTs and CTs) integrated into the system. The acquired data is then stored within the *MATLAB* environment. Next, to ensure uniform weighting for each dataset in the fault detection process, the collected data is subjected to normalization. The phase difference between the stator voltage and current occurs due to the time needed for magnetic fields to be established. Because of the motor's inductive nature, the current lags the voltage, causing a delay in the field response, which is a fundamental aspect of motor operation. This paper attempts to focus on synchronizing the impact of bearing faults on the IFMV and IFMC signals. It provided a more accurate estimation of the bearing fault signal, effectively enhancing the SNR in an automated manner. The synchronization is achieved by time shifting the IFMV signal as much as the existing phase difference (α) between voltage and current. Subsequently, subtracting the synchronized IFMV signal from the IFMC is expected to amplify the

bearing fault effects (magnitude) at the fault characteristic frequency due to synchronization, while reducing the effects of any components unrelated to the fault frequency (noise). Through this process, the SNR in the proposed novel residue signal termed the "synchronized deviation of instantaneous frequency of voltage and current" ΔIF, is enhanced. In the absence of a fault, the residue remains close to zero, while the presence of a fault causes it to deviate from zero. The selection of an appropriate residue is crucial, as it plays a key role in both detecting the presence or absence of a fault and determining its location. Subsequently, after acquiring the residue signal, the fault signatures for a faulty bearing can be revealed through spectral analysis, typically utilizing a straightforward FFT.
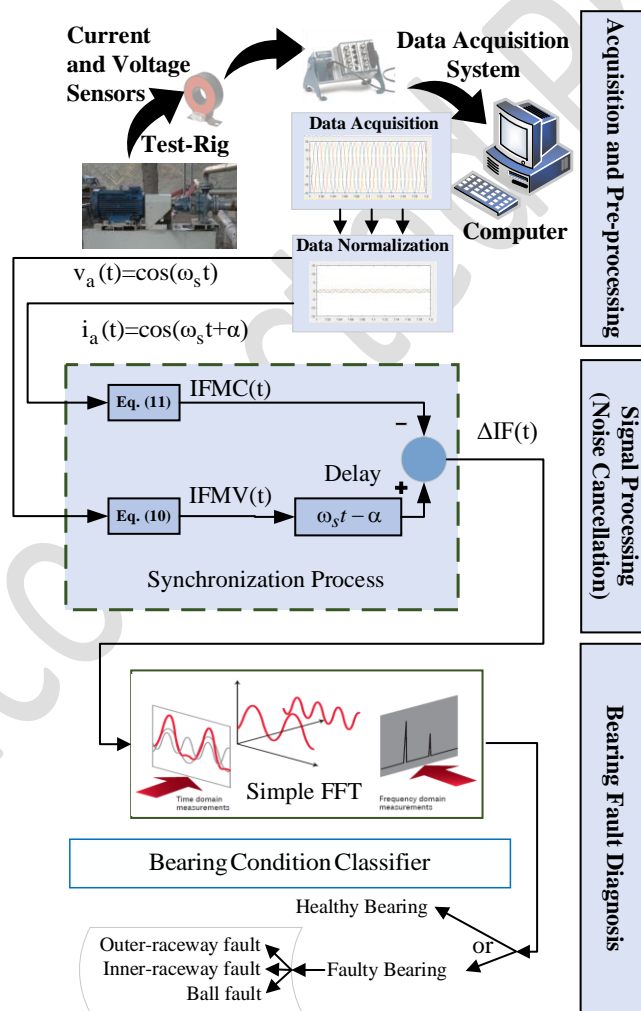

Fig. 3. General framework of the proposed method for diagnosing bearing faults

3- Simulation Results

A simulation test was conducted to ascertain the presence of fault signatures and reduce Gaussian noise in the spectral analysis of the proposed residue for a faulty bearing in an IM, as depicted in Fig. 4. This simulation was carried out using the *Simpower* toolbox in *MATLAB*. Following the methodology outlined in [1], a series of impulsive disturbances were introduced to the load torque to replicate a single-point bearing fault. This specific test employed a typical squirrel-cage IM, utilizing a star connection for the stator windings. The motor's characteristics are outlined in Table 1. The IM was connected to a three-phase voltage source with a line impedance of $z = 1 + j0.3\Omega$.
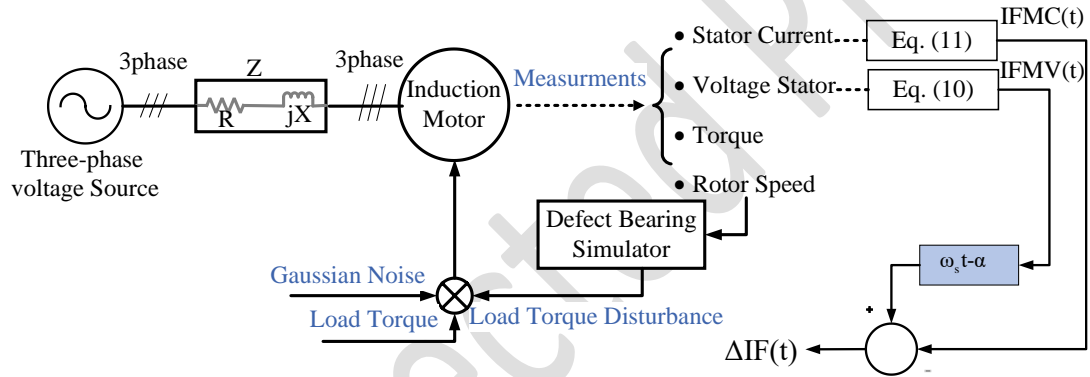

Fig. 4. Simulation of the influence of bearing faults on an IM and the generation of the proposed residue signal.

Considering that all experimental data discussed in Section IV were obtained from bearings of type 6309, the same bearing type was used for the simulation test. Consequently, the fault frequencies for this bearing type were determined as $F_O = 3.06 \times F_R$, $F_I = 4.95 \times F_R$, and $F_B = 2.00 \times F_R$. Assuming the IM operates at 1430 rpm (corresponding to $F_R = 23.84$ Hz), the fault frequency for the outer raceway, for example, translates to $F_O = 3.06 \times F_R = 72.98$ Hz. As depicted in Fig. 4, by measuring the rotor speed, a periodic impulsive function proportional to the fault signature of the outer raceway bearing is generated and then introduced into the load torque. Fig. 5 illustrates the load torque and standard *Gaussian* background noise for the bearing with an outer raceway fault. A constant load torque component of 50

N·m has also been considered. The amplitudes of the impulsive torque disturbances follow a *Gaussian*

distribution with a mean and standard deviation of 30 and 5, respectively.

Table 1. Properties of the IM used in Fig. 4

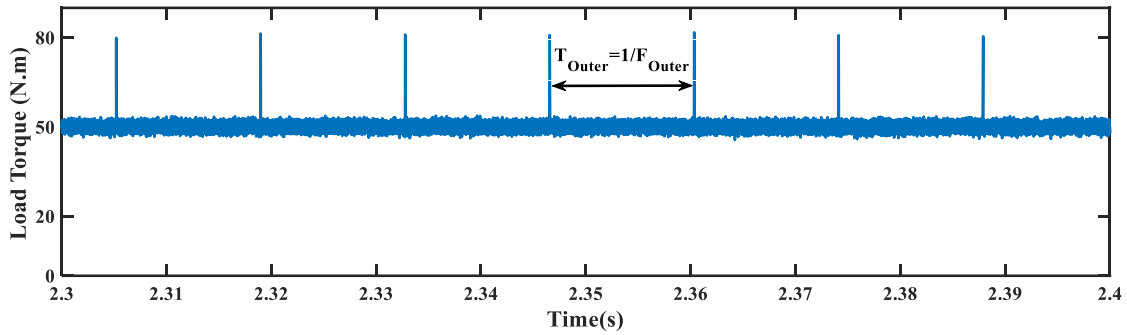| Symbol	Quantity	Value
P_n	nominal power	7.5kW
f_s	frequency	50Hz
V_{L-L}	voltage (line-line)	380V$_{rms}$
R_s	stator resistance	0.7384Ω
L_s	stator inductance	3.045mH
L_m	mutual inductance	124.1mH
R_r'	rotor resistance	0.7402Ω
L_r'	rotor inductance	3.045mH
J	inertia	0.0343J (kg.m^2)
F	friction factor	0.000503 N.m.s
P	pole pairs	2

Fig. 5. Load torque for a bearing with an outer raceway fault.

The simulation results of the spectral analysis for an IM with a bearing featuring an outer raceway fault

are presented in Fig. 6. As depicted in Fig. 6, the spectral analysis of IFMV and IFMC shows no

noticeable effects from characteristic fault frequencies or other non-fault components, such as twice the

frequency of the power supply ($2 \times f_s$). However, within the spectrum of the proposed residue signal, the

characteristic fault frequency is distinguishable. By comparing the vertical axis scale ranges of Fig. 6(a)

and Fig. 6(b) with Fig. 6(c), it becomes evident that the magnitudes of both fault and non-fault frequency

components are considerably lower than the level of Gaussian noise. This explains why in spectra Fig.

6(a) and Fig. 6(b), the fault component is not easily detectable. Nevertheless, the proposed method

effectively reduces both *Gaussian* noise signals through the synchronization of IFMV with IFMC and their subtraction. This substantially enhances the SNR value in the proposed signal, making it readily noticeable in the spectrum presented in Fig. 6(c).
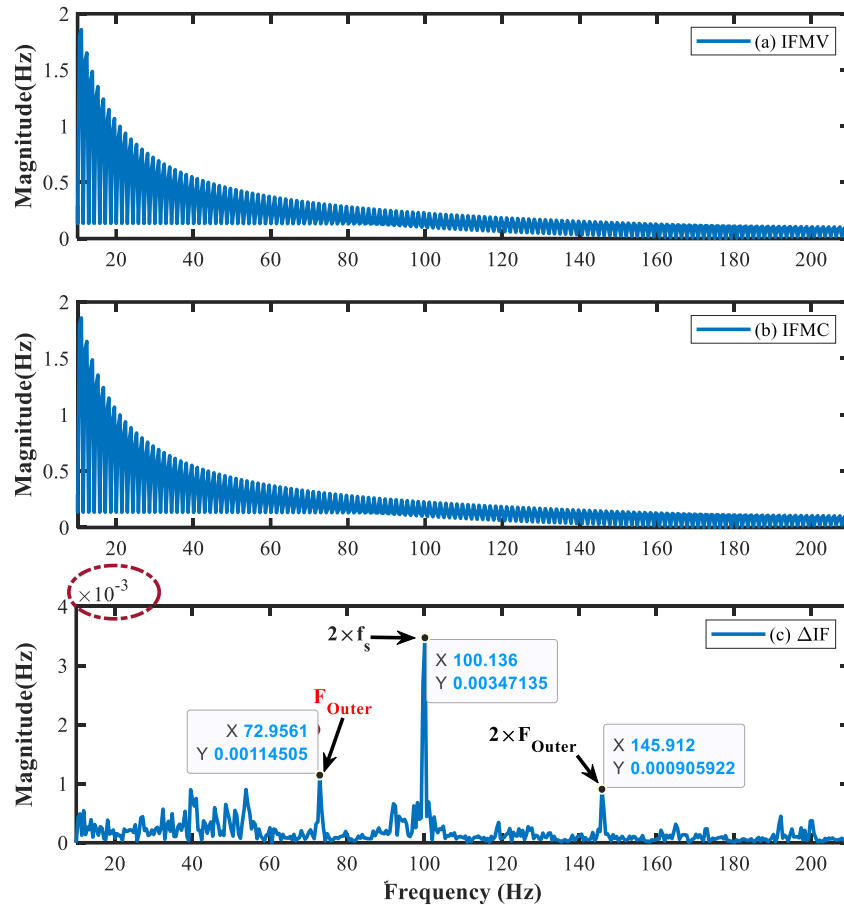

Fig. 6. Simulation results of spectral analysis for an outer raceway bearing fault - a comparison between (a) IFMV, (b) IFMC, and (c) the proposed residue signal (ΔIF).

4- Evaluation and Validation via Experimental Testing

4-1- Experimental Data Compilation

To evaluate the effectiveness of the suggested method in diagnosing bearing faults, we utilized a dataset obtained from an experimental setup illustrated in Fig. 7. This setup included an IM coupled with a centrifugal pump acting as the load device. The specifications of the IM and pump system are provided in

[1], and the pump is operated using water as the working fluid. A rigid coupling was employed to connect the motor and pump, ensuring consistent and reliable torque transmission during the tests. A custom-designed data acquisition systems were employed to capture stator current and voltage. IM voltage signals were captured using advanced National Instruments (NI) modules. For voltage measurements, the "NI 9225 300Vrms" module was used, which is specifically designed for three-phase systems and can handle line-to-neutral voltages up to 300Vrms. This module was particularly suitable for the 380Vrms power grid of the IM, enabling precise line-to-neutral voltage assessments. Two 50/5 CTs were employed to step down two of the stator currents for safe measurement using the module, while the third current waveform was computed in MATLAB using Kirchhoff's current law. The signals from the CTs were transmitted to a laptop through the "NI 9227" module, which was integrated into an "NI Compact DAQ" data acquisition chassis. Data sampling was performed at a high frequency of 51.2 kHz over 40 seconds for each test case. All acquired data were stored and processed using MATLAB [1].

The primary focus of this investigation was on real faults occurring in SKF ball bearings with specifications given in [1], specifically the 6309 type. The tests considered various fault types and sizes, including outer raceway faults (1 mm and 2 mm), inner raceway faults (1 mm), and ball faults (1 mm). These faults were artificially induced to simulate real-world conditions and assess the robustness of the proposed fault diagnosis method. To ensure comprehensive evaluation, the dataset was expanded to cover three distinct operational modes, where the motor was tested at 80%, 65%, and 50% of its rated current. During these tests, the motor speed varied between 2908 and 2957 rpm, representing typical operating conditions. Subsequently, the proposed method was applied to the dataset extracted from the three-phase voltages and currents of the IM's stator, encompassing 14 distinct operating conditions. These experimental scenarios have been succinctly summarized in Table 2. The scenarios are classified into 4 categories: healthy (C_1), outer raceway (C_2-C_7), inner raceway (C_8-C_{10}), and ball (C_{11}-C_{13}) faults. Test 14 is a double fault (simultaneous inner and outer raceway faults). This diverse set of experimental conditions provided a comprehensive foundation for validating the proposed method. The extracted

dataset included three-phase voltages and currents of the IM stator, capturing a wide range of fault
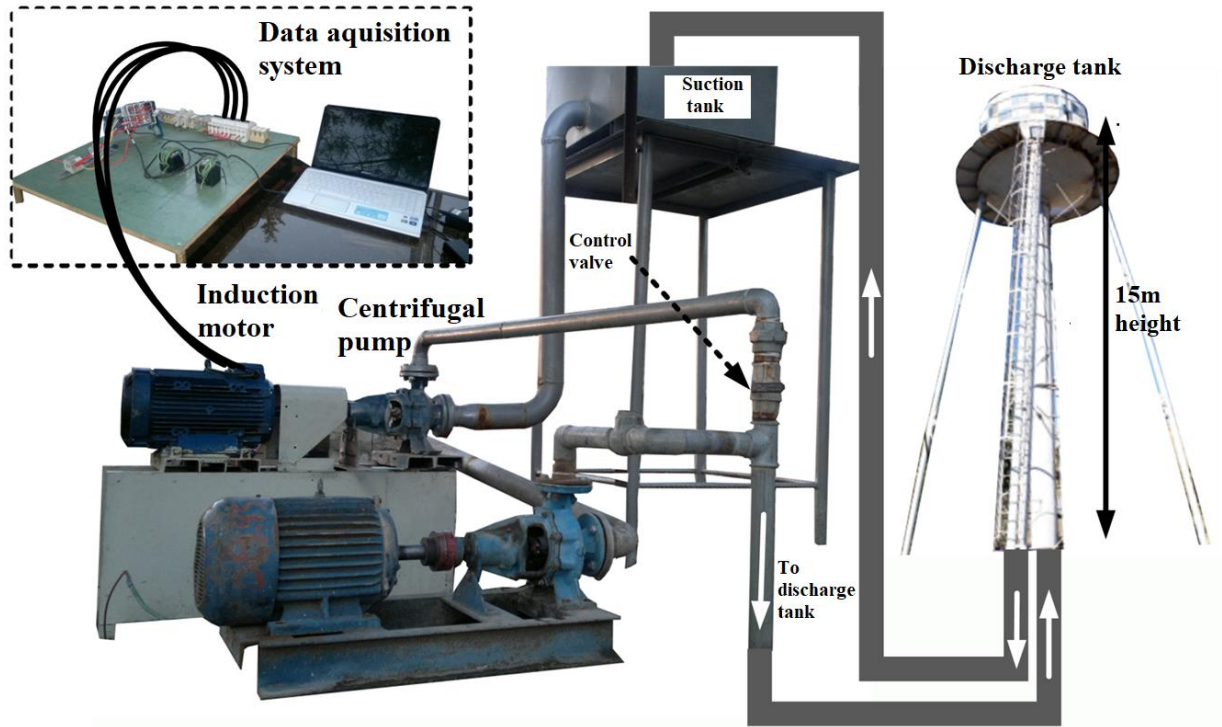
scenarios and operating conditions.

Fig. 7. Test rig and data collection system enclosed within the measurement panel for experimental validation [1].

Table 2. Bearing Conditions

Bearing Condition	Load percentage	label
Healthy	80	C_1
Outer raceway fault with a size of 2mm	80	C_2
Outer raceway fault with a size of 2mm	65	C_3
Outer raceway fault with a size of 2mm	50	C_4
Outer raceway fault with a size of 1mm	80	C_5
Outer raceway fault with a size of 1mm	65	C_6
Outer raceway fault with a size of 1mm	50	C_7
Inner raceway fault with a size of 1mm	80	C_8
Inner raceway fault with a size of 1mm	65	C_9
Inner raceway fault with a size of 1mm	50	C_{10}
Ball fault with a size of 1mm	80	C_{11}
Ball fault with a size of 1mm	65	C_{12}
Ball fault with a size of 1mm	50	C_{13}
Double faults (simultaneous inner and outer raceway faults)	65	C_{14}

4-2- Diagnosing Faults in the Outer Raceway

To evaluate the effectiveness of the proposed bearing fault diagnosis method, the FFT technique is applied. Practical experiments are conducted to assess the functionality of this proposed approach. These tests involve subjecting the IM to conditions in which faulty bearings are present, all under varying load conditions corresponding to different percentages of the rated current (80%, 65%, and 50%).

For high-level outer raceway faults (C_2-C_4), a 2mm outer raceway fault, the IM operates at 80%, 65%, and 50% of its rated current, with a shaft speed of 2919, 2937, and 2951 rpm (C_2: F_R=48.65Hz, C_3: F_R=48.95Hz, and C_4: F_R=49.19Hz). expected spikes are anticipated at F_{Outer}=148.87Hz, F_{Outer}=149.78Hz, and F_{Outer}=150.53Hz, respectively. The spectra depicted in Fig. 8 (c, f, and i), obtained using the proposed residue signal (ΔIF), illustrate the bearing fault diagnosis process for these fault conditions. The observed fault signatures on the spectra align closely with the calculated outer raceway fault signatures at 148.83Hz, 149.15Hz, and 151.07Hz, respectively.

As discussed in Section III, the core aim of the proposed method is to systematically reduce noise and enhance the SNR. As evident from the frequency spectrum comparison of the IFMV, IFMC, and ΔIF signals in all three tests from C_2 to C_4, the proposed signal (ΔIF) can significantly reduce the Gaussian noise present in both IFMV and IFMC signals by synchronizing the effects of bearing faults existing in these signals and subtracting them from each other. This noise reduction is so effective that fault frequencies, previously concealed within the background noise due to their low magnitude, become visible in the frequency spectrum of the proposed signal. Even in the case of test C_4, where the motor operates at 50% of its rated current and the fault characteristic frequency is close to the third harmonic frequency of the power grid ($3 \times f_s$), the proposed signal successfully unveils the fault frequency to a significant extent.
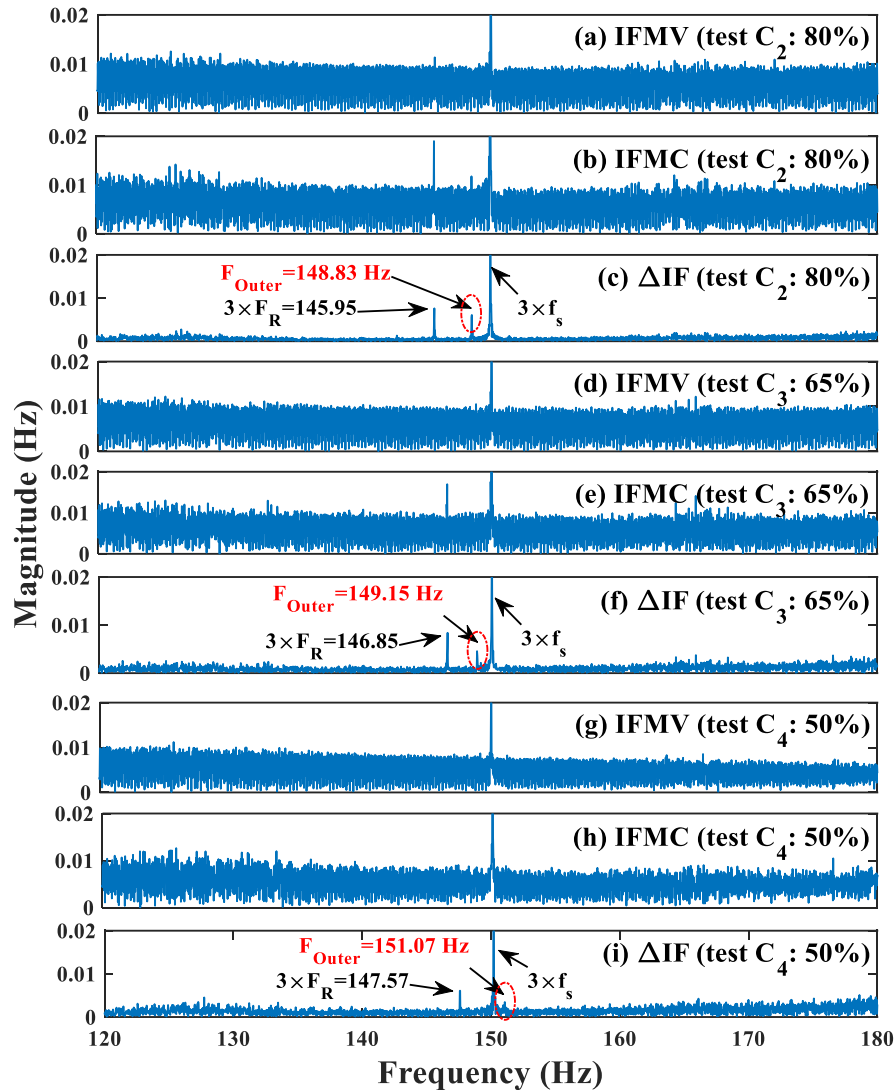
Fig. 8. Spectral analysis of IFMV, IFMC, and ΔIF (the proposed signal) for high-level outer raceway fault: (a-c) 80% of the rated current, (d-f) 65% of the rated current, and (g-i) 50% of the rated current (tests C_2-C_4).

Moving on to the examination of low-level outer raceway faults (C_5-C_7), the objective is to assess the method's capability to detect less severe faults within the outer raceway. In this scenario, a deliberately introduced 1mm-sized fault replaces the previous 2mm fault in a separate bearing. Data collection occurs as the IM operates at 80%, 65%, and 50% of its rated current. In Fig. 9, which focuses on the frequency range of 120Hz-180Hz, the anticipated fault signatures in all three spectra become apparent. A visual examination of this figure highlights the effectiveness of the proposed method, as the outer raceway fault

signatures are clearly and prominently distinguishable. This indicates the method's robustness in detecting

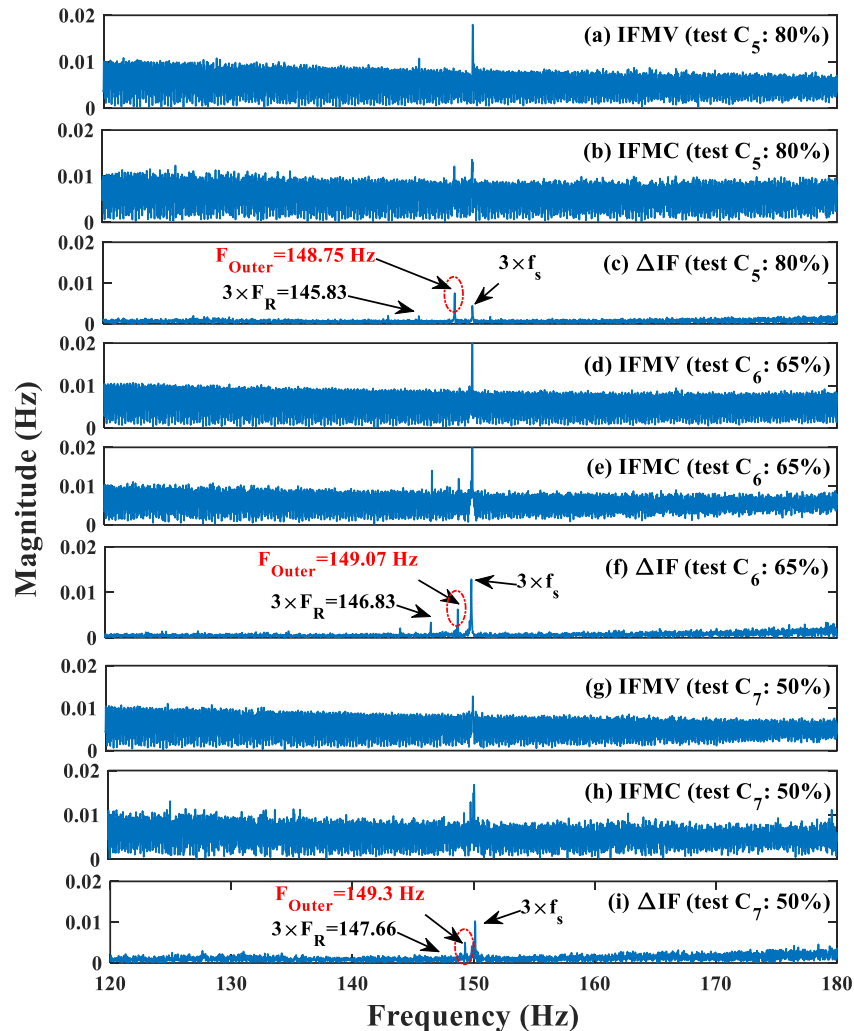even subtle faults under varying operating conditions.

Fig. 9. Spectral analysis of IFMV, IFMC, and ΔIF (the proposed signal) for low-level outer raceway fault: (a-c) 80% of the rated current, (d-f) 65% of the rated current, and (g-i) 50% of the rated current (tests C_5-C_7).

4-3- Diagnosing Faults in the Inner Raceway and Ball

In an additional experimental scenario, single-point faults with a magnitude of 1mm were introduced on

both the inner raceway (C_8-C_{10}) and the ball (C_{11}-C_{13}) of the bearing. The rotational frequencies for these

tests are detailed as follows: C_8 (F_R=48.48Hz), C_9 (F_R=48.85Hz), C_{10} (F_R=49.17Hz), C_{11} (F_R=48.61Hz),

C_{12} (F_R=48.85Hz), and C_{13} (F_R=49.22Hz). As a result, it is expected that spikes will appear at

F_{Inner}=239.54Hz, 241.77Hz, 243.34Hz, and F_{Ball}=97.22Hz, 97.70Hz, and 98.44Hz, respectively. To facilitate a more reader-friendly interpretation, Figs. 10(a-i) and 11(a-i) have been incorporated to illustrate the spectrum of the proposed residue signal in comparison with the IFMV and IFMC signals for conditions (C_8-C_{10}) and (C_{11}-C_{13}), respectively.
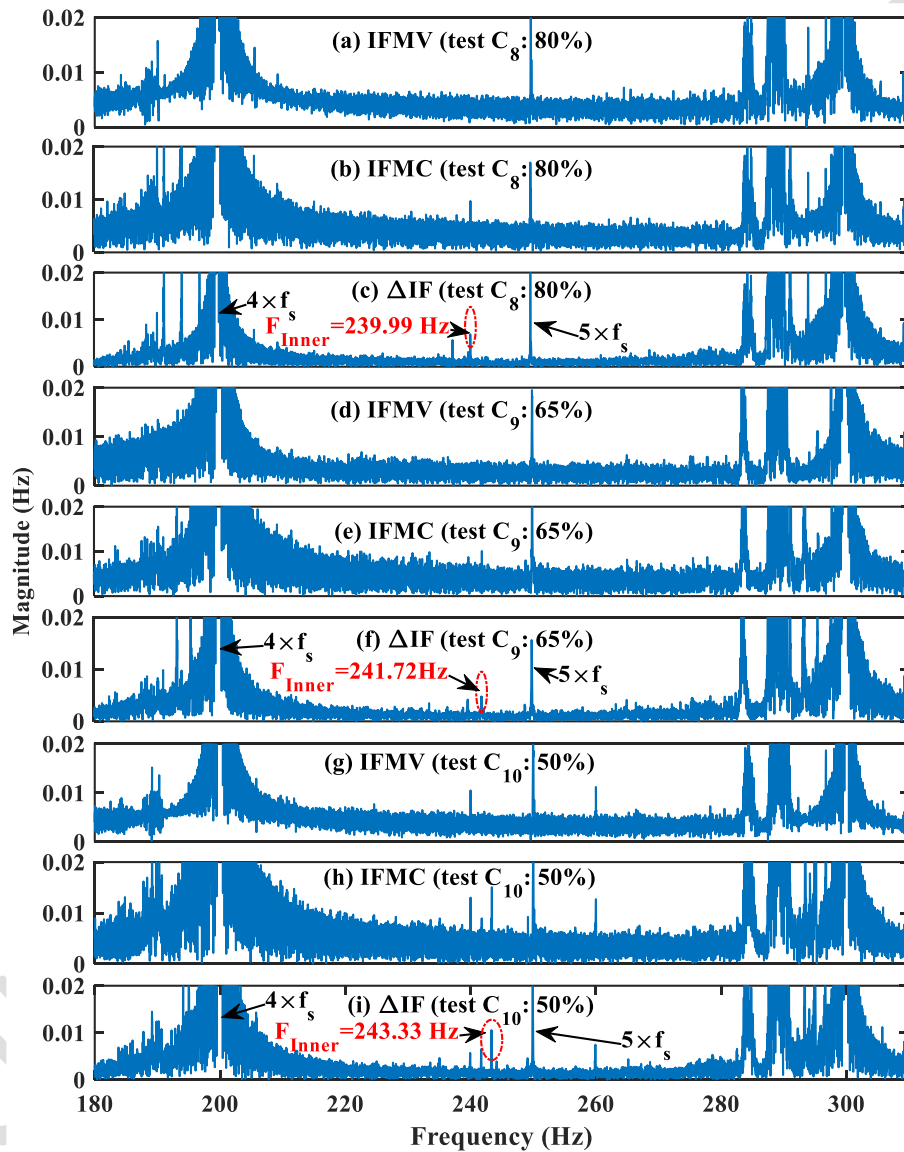

Fig. 10. Spectral analysis of IFMV, IFMC, and ΔIF (the proposed signal) for inner raceway fault: (a-c) 80% of the rated current, (d-f) 65% of the rated current, and (g-i) 50% of the rated current (tests C_8-C_{10}).

Upon analysis of the presented figures, it is evident that the fault frequencies derived from the proposed residual signal (ΔIF) are measured at 239.99Hz, 241.72Hz, and 243.34Hz for the inner raceway faults (C_8-C_{10}), and 97.22Hz, 97.68Hz, and 98.41Hz for the ball faults (C_{11}-C_{13}). Importantly, these recorded frequencies closely align with the calculated inner raceway and ball fault frequencies. Notably, in this scenario, neither the inner raceway fault frequency nor the ball fault is discernible within the spectrum of the IFMV and IFMC signals. Only the IFMV signal accurately displays the ball fault frequency. However, upon a meticulous comparison between the IFMV signal and the spectrum of the proposed residual signal (Fig. 10 (a with c), (d with f), and (g with i)), it becomes apparent that the proposed method has effectively mitigated Gaussian noise interference in the ball fault tests, thereby showcasing the method's ability to enhance fault detection under challenging conditions.

4-4- Diagnosing Double Faults

In practical scenarios, it is possible for a bearing to experience multiple faults simultaneously, such as a combination of outer raceway and inner raceway defects, or ball defects occurring alongside raceway damage. Diagnosing such "double faults" better demonstrates the effectiveness of a fault diagnosis method. To address this, a special test has been performed considering the simultaneous presence of inner and outer ring faults in the bearing (test C_{14}). The rotational frequency for this test is F_R=48.96Hz. Consequently, spectral analysis is expected to reveal spikes at F_{Inner}=242.35Hz, and F_{Outer}=149.82Hz. To demonstrate this, Fig. 12 has been included, showing the spectrum of the proposed residual signal alongside the IFMV and IFMC signals. As it is clear, the proposed residual signal has been able to reveal both fault components in the frequency spectrum with good approximation.
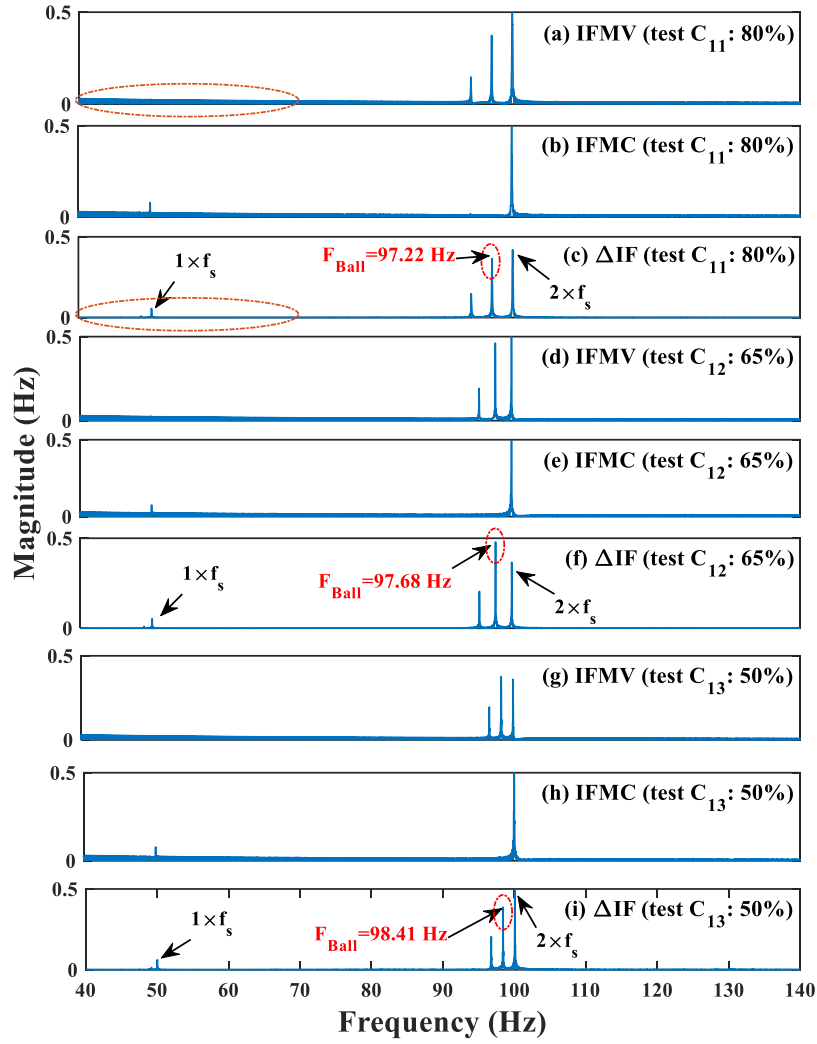
Fig. 11. Spectral analysis of IFMV, IFMC, and ΔIF (the proposed signal) for ball fault: (a-c) 80% of the rated current, (d-f) 65% of the rated current, and (g-i) 50% of the rated current (tests C_{11}-C_{13}).
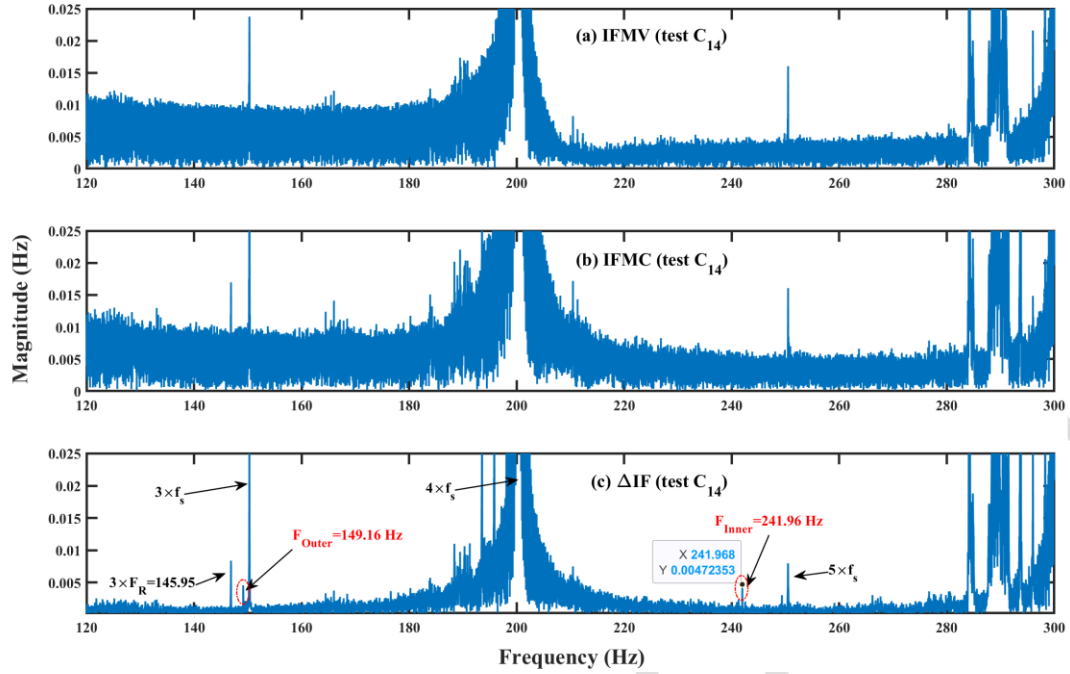
Fig. 12. Spectral analysis of IFMV, IFMC, and ΔIF (the proposed signal) for double faults: the simultaneous existence of inner and outer raceway faults in the bearing (test C_{14}): (a) IFMV, (b) IFMC, and (c) ΔIF.

5- Appendix

$$z = k_1 \frac{L_m r_r'}{(L_{l_r} + L_m)}$$

$$G = -\omega_s \left(I_m (L_{l_s} + 1) + \frac{(L_{l_r}' + L_m)\omega_s^2 L_m I_m}{(L_{l_r}' + L_m)^2 \omega_s^2 + r_r'^2} \right)$$

$$H = r_s I_m - \frac{L_m I_m \omega_s^2 r_r'}{(L_{l_r}' + L_m)^2 \omega_s^2 + r_r'^2}$$

$$I = -(\omega_s - \omega_f)\left(I_1 (L_{l_s} + 1) + \frac{(L_{l_r}' + L_m)L_m I_1 (\omega_s - \omega_f)^2}{1 - (L_{l_r}' + L_m)^2 (\omega_s - \omega_f)^2} \right)$$

$$J = r_s I_1 - \frac{r_r' L_m I_1 (\omega_s - \omega_f)^3}{1 - (L_{l_r}' + L_m)^2 (\omega_s - \omega_f)^2}$$

$$K = -(\omega_s + \omega_f)\left(I_1 (L_{l_s} + 1) + \frac{L_m I_1 (\omega_s + \omega_f)^2 (L_{l_r}' + L_m)}{(L_{l_r}' + L_m)^2 (\omega_s + \omega_f)^2 + r_r'^2} \right)$$

$$L = r_s I_1 - \frac{r_r' L_m I_1 (\omega_s + \omega_f)^2}{(L_{l_r}' + L_m)^2 (\omega_s + \omega_f)^2 + r_r'^2}$$

$$\begin{cases} M = (G^2 + H^2)\omega_s + (I^2 + J^2)(\omega_s - \omega_f) + (K^2 + L^2)(\omega_s + \omega_f) \\ M' = I_m^2 \omega_s + I_1^2 (\omega_s - \omega_f) + I_1^2 (\omega_s + \omega_f) \end{cases}$$

$$\begin{cases} N = (GI + JH)(2\omega_s - \omega_f) \\ N' = I_m I_1 (2\omega_s - \omega_f) \end{cases}$$

$$\begin{cases} O = (GK + HL)(2\omega_s + \omega_f) \\ O' = I_m I_1 (2\omega_s + \omega_f) \end{cases}$$

$$\begin{cases} P = (KI + LJ)(2\omega_s) \\ P' = I_1^2 (2\omega_s) \end{cases}$$

$$R = (JK - LI)(2\omega_s)$$

$$Q = (GJ - HL)(2\omega_s - \omega_f) + (HK - GL)(2\omega_s + \omega_f)$$

$$\begin{cases} d(t) = a + b\cos((2\omega_s - \omega_f)t + 2\alpha) + c\cos((2\omega_s + \omega_f)t + 2\alpha) \\ \qquad + d\cos(2\omega_s t + 2\alpha) + e\sin\omega_f t + f\sin 2\omega_f t \\ d'(t) = a' + b'\cos((2\omega_s - \omega_f)t) + c'\cos((2\omega_s + \omega_f)t) \\ \qquad + d'\cos 2\omega_s t \end{cases}$$

where:

$$\begin{cases} a = (G^2 + H^2) + (I^2 + J^2) + (K^2 + L^2) \\ a' = I_m^2 + 2I_1^2 \end{cases}$$

$$\begin{cases} b = 2(GI + GH) \\ b' = 2I_m I_1 \end{cases}$$

$$\begin{cases} d = 2(KI + LJ) \\ d' = 2I_1^2 \end{cases}$$

$$e = 2(G(J - L) + H(K - I))$$

$$f = 2(JK - LI).$$

6- Conclusion

In this paper, we have addressed a significant challenge in the domain of bearing fault diagnosis, with a particular focus on detecting subtle or early-stage defects in IMs. The conventional approach of analyzing current signals often encounters issues related to noise interference, leading to difficulties in accurately identifying fault characteristic frequencies. To overcome this challenge, we have introduced an innovative noise cancellation technique based on the synchronized deviation of instantaneous frequency of voltage and current. The proposed method represents a promising solution to the persistent problem of noise interference that has historically hindered accurate bearing fault diagnosis. The results obtained from both simulation and real-world experiments validate the effectiveness of this approach in identifying faults within the outer/inner raceways and ball faults.

By successfully reducing noise components, this method significantly enhances the precision and reliability of bearing fault diagnosis in the context of IMs. Consequently, it has the potential to make a substantial impact on the field of machinery maintenance and operational efficiency by facilitating early detection and intervention in bearing faults. This, in turn, can lead to a reduction in downtime and minimize costly breakdowns. The advancement presented in this paper holds the promise of not only improving the overall performance but also extending the longevity of industrial machinery, contributing to the broader goals of efficiency and reliability in industrial operations. In conclusion, this study provides a novel and effective approach to bearing fault diagnosis in IMs, with practical implications for the maintenance of industrial machinery.

7- Nomenclature

IM	Induction motor
FFT	Fast Fourier transform
SCRS	Synchronized current residue square
SNR	Signal-to-noise ratio
IFMV	Instantaneous frequency of the motor voltage
IFMC	Instantaneous frequency of the motor current

References

[1] S. Nazari, S. Shokoohi, J. Moshtagh, A Current Noise Cancellation Method Based on Integration of Stator Synchronized Currents for Bearing Fault Diagnosis, IEEE Transactions on Instrumentation and Measurement, (2023) 1-1.

[2] F. Dalvand, S. Dalvand, F. Sharafi, M. Pecht, Current noise cancellation for bearing fault diagnosis using time shifting, IEEE Transactions on Industrial Electronics, 64(10) (2017) 8138-8147.

[3] K. Xu, X. Song, A Current Noise Cancellation Method Based on Fractional Linear Prediction for Bearing Fault Detection, Sensors, 24(1) (2023) 52.

[4] B. Guan, X. Bao, H. Qiu, D. Yang, Enhancing bearing fault diagnosis using motor current signals: A novel approach combining time shifting and CausalConvNets, Measurement, 226 (2024) 114049.

[5] M. Sun, H. Wang, P. Liu, Z. Long, J. Yang, S. Huang, A novel data-driven mechanical fault diagnosis method for induction motors using stator current signals, IEEE Transactions on Transportation Electrification, 9(1) (2022) 347-358.

[6] W. Zhou, T.G. Habetler, R.G. Harley, Bearing Fault Detection Via Stator Current Noise Cancellation and Statistical Control, IEEE Transactions on Industrial Electronics, 55(12) (2008) 4260-4269.

[7] R.R. Schoen, T.G. Habetler, F. Kamran, R.G. Bartfield, Motor bearing damage detection using stator current monitoring, IEEE Transactions on Industry Applications, 31(6) (1995) 1274-1279.

[8] M. Arkan, H. Çaliş, M. Tağluk, Bearing and misalignment fault detection in induction motors by using the space vector angular fluctuation signal, Electrical Engineering, 87(4) (2005) 197-206.

[9] A. Bouras, S. Bennedjai, S. Bouras, Experimental detection of defects in variable speed fan bearing using stator current monitoring, SN Applied Sciences, 2 (2020) 1-8.

[10] F.B. Abid, S. Zgarni, A. Braham, Distinct bearing faults detection in induction motor by a hybrid optimized SWPT and aiNet-DAG SVM, IEEE Transactions on Energy Conversion, 33(4) (2018) 1692-1699.

[11] S. Singh, N. Kumar, Detection of bearing faults in mechanical systems using stator current monitoring, IEEE Transactions on Industrial Informatics, 13(3) (2016) 1341-1349.

[12] V.C. Leite, J.G.B. da Silva, G.F.C. Veloso, L.E.B. da Silva, G. Lambert-Torres, E.L. Bonaldi, L.E.d.L. de Oliveira, Detection of localized bearing faults in induction machines by spectral kurtosis and envelope analysis of stator current, IEEE Transactions on Industrial Electronics, 62(3) (2014) 1855-1865.

[13] F. Immovilli, M. Cocconcelli, A. Bellini, R. Rubini, Detection of generalized-roughness bearing fault by spectral-kurtosis energy of vibration or current signals, IEEE Transactions on Industrial Electronics, 56(11) (2009) 4710-4717.

[14] X. Zhang, Y. Liang, J. Zhou, A novel bearing fault diagnosis model integrated permutation entropy, ensemble empirical mode decomposition and optimized SVM, Measurement, 69 (2015) 164-179.

[15] W. Zhou, B. Lu, T.G. Habetler, R.G. Harley, Incipient bearing fault detection via motor stator current noise cancellation using wiener filter, IEEE Transactions on Industry Applications, 45(4) (2009) 1309-1317.

[16] M.E.H. Benbouzid, M. Vieira, C. Theys, Induction motors' faults detection and localization using stator current advanced signal processing techniques, IEEE Transactions on power electronics, 14(1) (1999) 14-22.

[17] M. Pineda-Sanchez, R. Puche-Panadero, M. Riera-Guasp, J. Perez-Cruz, J. Roger-Folch, J. Pons-Llinares, V. Climente-Alarcon, J.A. Antonino-Daviu, Application of the Teager–Kaiser energy operator to the fault diagnosis of induction motors, IEEE Transactions on energy conversion, 28(4) (2013) 1036-1044.

[18] F. Dalvand, M. Kang, S. Dalvand, M. Pecht, Detection of Generalized-Roughness and Single-Point Bearing Faults Using Linear Prediction-Based Current Noise Cancellation, IEEE Transactions on Industrial Electronics, 65(12) (2018) 9728-9738.

[19] X. Wang, Z. Liu, M. Dai, W. Li, J. Tang, Time-shift denoising Combined with DWT-Enhanced Condition Domain Adaptation for Motor Bearing Fault Diagnosis via Current Signals, IEEE Sensors Journal, (2024).

[20] X. Wang, R. Meng, G. Wang, X. Liu, X. Liu, D. Lu, The research on fault diagnosis of rolling bearing based on current signal CNN-SVM, Measurement Science and Technology, 34(12) (2023) 125021.

[21] S. Shokoohi, J. Moshtagh, Beyond Signal Processing: A Model-Based Luenberger Observer Approach for Accurate Bearing Fault Diagnosis, AUT Journal of Electrical Engineering, (2024) -.

[22] A. Ibrahim, M. El Badaoui, F. Guillet, F. Bonnardot, A new bearing fault detection method in induction machines based on instantaneous power factor, IEEE Transactions on Industrial Electronics, 55(12) (2008) 4252-4259.

[23] F. Dalvand, A. Kalantar, M.S. Safizadeh, A Novel Bearing Condition Monitoring Method in Induction Motors Based on Instantaneous Frequency of Motor Voltage, IEEE Transactions on Industrial Electronics, 63(1) (2016) 364-376.

[24] F. Dalvand, A. Kalantar, S. Shokoohi, H. Bevrani, Time-domain bearing condition monitoring in induction motors using instantaneous frequency of motor voltage, in: 2014 Smart Grid Conference (SGC), 2014, pp. 1-7.

[25] J.R. Stack, T.G. Habetler, R.G. Harley, Fault classification and fault signature production for rolling element bearings in electric machines, in: 4th IEEE International Symposium on Diagnostics for Electric Machines, Power Electronics and Drives, 2003. SDEMPED 2003., 2003, pp. 172-176.